processes

MDPI

Article

Structure Size Optimization and Internal Flow Field Analysis of a New Jet Pump Based on the Taguchi Method and Numerical Simulation

Zhiliang Wang [1,2], Yu Lei [2,3], Zhenhua Wu [2,3], Jian Wu [2,3], Manlai Zhang [2,4] and Ruiquan Liao [1,2,*]

1 School of Petroleum Engineering, Yangtze University, Wuhan 430100, China
2 Lift Test Base of China National Petroleum Corporation, Hami 839009, China
3 Research and Development Center, Tuha Oilfield Company, China National Petroleum Corporation, Hami 839009, China
4 School of Mechanical Engineering, Yangtze University, Jingzhou 434023, China
* Correspondence: zhiliang-wang1996@foxmail.com

Abstract: Interlayer contradiction (high-pressure oil that prevents low-pressure oil from being extracted) has always been the main factor affecting the oil-recovery efficiency of the many oil-bearing series in shale oil wells in Eastern Shandong, China. If steps to deal with interlayer contradiction are not taken, Shengli Oilfield's oil-recovery efficiency will be significantly reduced after a certain period of exploitation. Furthermore, as the drilling depth increases, the formation-fluid supply capacity of Shengli Oilfield becomes worse and further increases the difficulty of oil recovery as well as production costs. In order to improve the oil-recovery efficiency of shale oil wells in Eastern Shandong and realize cost reductions and efficiency increases, we designed a new jet pump in this study. The pump can be used for oil recovery according to the principle of Venturi jet propulsion, as the required power fluid is not a high-pressure fluid injected from the ground, but rather high-pressure oil that is present in the formation. Through the analysis of the overall structure of the new jet pump, it was found that the pump could not only transform the existing interlayer contradiction (co-mining of high and low oil layers by utilizing interlayer contradiction), but also had the characteristics of a simple structure and low production costs. Since the structural dimensions of the jet pump and the physical characteristic parameters of the fluid have significant impacts on pump efficiency, we first analyzed the internal flow field of the jet pump by using numerical simulations and found that the throat–nozzle distance, area ratio, throat length–diameter ratio, diffuser angle, and flow ratio had the most significant impacts on pump efficiency. After obtaining the specific numerical range of the abovementioned structural parameters when the pump efficiency was as its maximum, an orthogonal array designed according to the Taguchi method was used to conduct experiments. According to a range analysis and an analysis of variance, at an unchanged flow ratio (0.3156), the new jet pump achieved the highest efficiency (31.26%) when the throat–nozzle distance was 2.62 mm, the throat length was 46 mm, the throat diameter was 6.8 mm, and the diffuser angle was 7.5°. In comparing its efficiency with that before optimization, we noticed that the efficiency was significantly improved by about 10%. These research results not only offer a new idea for the existing oil-recovery mode, but also introduce a new method for optimizing the structure of jet pumps.

Keywords: Taguchi method; numerical simulation; new jet pump; structural size optimization; comparison and analysis

Citation: Wang, Z.; Lei, Y.; Wu, Z.; Wu, J.; Zhang, M.; Liao, R. Structure Size Optimization and Internal Flow Field Analysis of a New Jet Pump Based on the Taguchi Method and Numerical Simulation. *Processes* **2023**, *11*, 341. https://doi.org/10.3390/pr11020341

Academic Editor: Alfredo Iranzo

Received: 18 December 2022
Revised: 10 January 2023
Accepted: 10 January 2023
Published: 20 January 2023

1. Introduction

With the continuous development of domestic drilling and production technology, China's onshore drilling depth has been advancing from 4500–6000 m (deep wells) to 6000–9000 m (ultra-deep wells) [1,2]. It has been proven that there are a large number of unconventional oil reservoirs in Eastern Shandong. These reservoirs require artificial

lift technology [3,4] (mechanical devices sent down the shaft to replenish the energy of the fluid in the well by performing work on the fluid in the pipe) to aid in extracting oil from the wells because of the large buried depth and natural formation energy in the wells, which is insufficient to sustain their flow production [5]. We often use artificial lift systems with deep-well jet pumps [6,7] when extracting oil from unconventional reservoirs in the area. However, Shengli Oilfield has many oil-bearing series (multiple sections of oil layers with different levels of pressure in the wells), making interlayer contradiction more prominent. When extracting high-pressure oil and low-pressure oil in a well, high-pressure oil enters the low-pressure reservoir under the effect of its own pressure, preventing the recovery of low-pressure oil. In addition, after the extraction proceeds for some time, the oil pressure in the well significantly drops, which further impedes oil recovery and leads to a significant decline in the oil-lifting efficiency of the jet pump. Therefore, the following oil-recovery engineering problems in East China urgently require solutions: (1) the current oil-recovery efficiency of deep-well jet pumps needs to be improved, (2) the drilling and production costs need to be lowered, and (3) the amount of downhole safety accidents needs to be reduced.

To fully understand the basic theory [8,9], structural composition [10], and application effect of the jet pump [11], as well as to ensure safe on-site operations and to help decrease costs to increase efficiency, scholars at home and abroad have carried out a large amount of analysis and research on the jet pump. For example, Y.R. Reddy et al. [12] conducted a theoretical study on the efficiency of jet pumps. When the flow ratio was 1, they found that the maximum ideal pump effect of the jet pump was 50%, but the pump effect was only 39.4% after the structure of the jet pump was optimized using basic theory. When the appropriate material was chosen to reduce the friction resistance of the inner wall of the jet pump facing the fluid, the pump efficiency was able to reach more than 40%. K.E. Brown and H. Petrie jointly published *The Artificial Lift Method* [13], a book that systematically summarizes the principle, formula derivation, and application of the jet pump. However, their study was limited, as it assumed the two fluids in a jet pump have the same density. A. W. Grupping [14] elaborated on the working principle, the calculation formula, the curve of the working characteristic, the calculation program, and an example calculation of the oil-well jet pump, and they provided a set of theories and calculation methods combined with oil-production conditions. S.H. Winoto et al. [15] conducted a theoretical analysis and laboratory experiments on the efficiency of the jet pump and studied the impacts of the area ratio between the nozzle and throat pipe and the nozzle sections of different shapes on jet pump performance by using an experimental bench. Finally, they concluded that jet pumps with circular nozzles have the greatest pump efficiency. C.B. Wang [16] deduced the basic characteristic equation and efficiency of the jet pump using energy conservation and obtained an optimal parameter equation by choosing the multivariate function method to find the extreme value. After analyzing the friction loss coefficient and other parameters, he concluded that the friction loss coefficient directly affects the size of the optimal area ratio and indirectly affects the efficiency of the jet pump.

J. Thomson [11] was the first person to draw the structural diagram of the jet pump. Since then, more and more scholars have engaged in theoretical analysis, structural design, and research on the applications of jet pumps. O. B. Kwon [17] and other scholars used numerical simulations [18,19] and experiments to study the effects of the shape of the mixing chamber and different jet rates on the performance of jet pumps. After comparing simulation data with experimental data, it was found that the RNG k–ε model was more suitable to simulate the internal flow field of pumps than the standard k–ε model. If the flow rate is low, there will be some reverse flow in a pump. Y. Yamazaki [20] studied the influence of the shape of the nozzle (circular, notched, and flower-shaped) and the shape of the throat (traditional straight throat and diverging throat with a very gentle gradient) on the performance of jet pumps. The velocity distribution in the pipe and the local friction loss coefficient were experimentally analyzed, and the performance of the jet pumps was evaluated using these concrete values. During the experiment, the pump

efficiency of all jet pumps could be improved when the diverging throat with a very gentle gradient was selected and only the nozzle shape was changed. K. Aldaş et al. [21] used CFD to compare the performance of jet pumps with different levels of surface roughness. They found that the SST model could best improve simulation accuracy: when the area ratio was 5.92 and the relative roughness was 0.05, the relative pump efficiency decreased by about 60%. K Xu et al. [22] used CFD to numerically simulate an annular jet pump; after establishing an accurate RBF neural network model and an NSGA-II algorithm, the multiobjective optimization of the annular jet pump was carried out. By comparing a preoptimized jet pump with an optimized jet pump, it was found that the head ratio of the former was increased by 30.46% and the efficiency was slightly improved. Regarding the application of jet pumps, S. Chen et al. [23] developed an integrated sand-removal system that used a jet pump to remove sand particles in wells. After optimizing the design of the jet pump and applying the system in the field, they found that the jet pump could effectively remove loose sand and the system could effectively avoid loss circulation. C. C. Gao [24] analyzed the application of jet pump technology for environmental protection and found that jet pump technology has played a very important role in sewage treatment, waste gas treatment, dust treatment, and other treatments. S. Sarshar [25] analyzed the application of jet pumps in oil and gas production and found that jet pump technology cannot only improve the production of oil and gas wells and increase low gas pressure, but is also a relatively economical and simple production method. B. Sun [26] studied the exploitation of coalbed methane with a jet pump by conducting an analysis of the basic theory of jet pumps and experiments on the solid–liquid two-phase flow. Thus, this study created new jet pump technology that can be used to extract coalbed methane and was applied to 116 gas wells with improved results.

To summarize, although jet pumps have been studied for many years [8,9,27], the basic performance equations of jet pumps are still not unified [11] and some basic performance equations are not universal (the equations are only applicable when the two fluid densities in a jet pump are the same) [11,16]. Although deep-well jet pumps [6,7,14] have been widely used in oil recovery engineering [7,28], the power fluid currently used in pumps is manually injected high-pressure fluid, which leads to high production costs. In addition, when there are multiple reservoirs with different levels of pressure in a well, interlayer contradiction (high-pressure oil that hinders low-pressure oil recovery [29,30]) further increases the difficulty and cost of oil recovery. In order to improve oil recovery efficiency, effectively exploit low energy and low production layers, and better realize cost reduction and efficiency increases, this paper designed a new jet pump after comprehensively considering the characteristics of strata, production cost, and oil-recovery efficiency in Eastern Shandong, and the basic characteristic equation of this new kind of jet pump was derived by using a momentum equation, an energy equation, and a continuity equation (when the two fluid densities in a jet pump are different, this equation is also applicable). Compared with traditional jet pumps [6,7,16,28], the new jet pump can effectively transform interlayer contradiction and further achieve lower costs and a higher efficiency. Since pump efficiency is subject to structural dimensions and other factors, we first used numerical simulations to understand the main structural parameters influencing pump efficiency and the intervals of the main structural dimensions at maximum pump efficiency. Then, we optimized the structural dimensions of the new jet pump using the Taguchi method. Based on range and signal-to-noise ratio analyses, the order of impact of the throat diameter, diffuser angle, throat–nozzle distance, and throat length on pump efficiency was obtained. The specific contribution (relative influence on pump efficiency) of each control factor was also derived using an ANOVA. Ultimately, the specific throat–nozzle distance, throat diameter, and throat length needed for maximum pump efficiency were calculated.

2. The Structure and Working Principle of the New Jet Pump

The conventional tube-string structure currently used for commingled production in an oil well containing multiple reservoir sections (e.g., high- and low-pressure reservoirs)

is shown in Figure 1a. Although this method [8,9,31] can be used to extract high- and low-pressure oil, it presents a prominent contradiction between layers, causing the high-pressure oil to be pushed by its own pressure into the low-pressure reservoir, thus hindering the recovery of low-pressure oil. To reduce the difficulty of oil recovery and achieve lower costs and a higher efficiency, we propose an oil-recovery process with a new type of jet pump, whose overall tube-string structure is shown in Figure 1b. The new jet pump is installed between two packers such that the lower packer is located between the high-pressure reservoir and the low-pressure reservoir, whereas the upper packer is located above the new jet pump so that the low-pressure reservoir is separated from the other reservoirs.

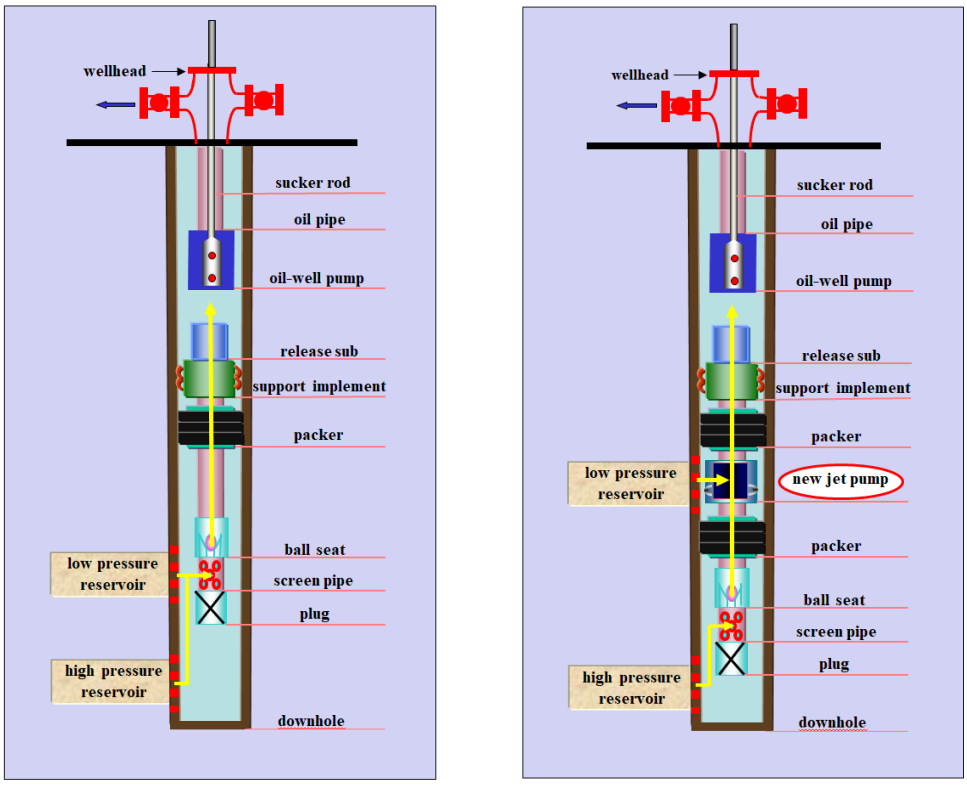

Figure 1. Comparison between a conventional co-production string and a co-production string with a deep-well jet pump. (**a**) Schematic diagram of a conventional co-production string. (**b**) Schematic diagram of a co-production string with a new jet pump.

Figure 2 shows the overall structure of the new jet pump. The tool is assembled from 25 parts, with an overall simple structure [32]. Under its own pressure, when high-pressure oil enters the jet pump along the internal flow path of the tube string (the orange arrow in Figure 2 indicates the flow direction of the high-pressure oil in the jet pump), the high-pressure fluid generates an entrainment effect through the nozzle jet flow due to the small internal flow channel of the nozzle in the pump. This forms a negative-pressure zone near the nozzle outlet, which, combined with the pressure difference, causes low-pressure fluid (the green arrow in Figure 2 indicates the flow direction of the low-pressure fluid in the jet pump) to enter the tool through the small hole on the short joint of the shell and then pass through the check valve along the flow path to the negative-pressure zone. At this time, only a small amount of the two fluids is mixed. The full mixture is achieved in the throat. When the mixture (the red arrow in Figure 2 indicates its flow direction) enters the diffuser tube, part of its kinetic energy is converted by the expanding flow path (a gradually expanding path along the central flow channel of the diffuser tube) into pressure energy, thus effectively increasing the oil pressure in the low-pressure reservoir. When the mixture enters the oil-well pump along the connected oil-tube string, the plunger inside

the oil-well pump lifts the mixture to the ground through an up-and-down reciprocating motion, achieving the simultaneous extraction of high- and low-pressure oil.

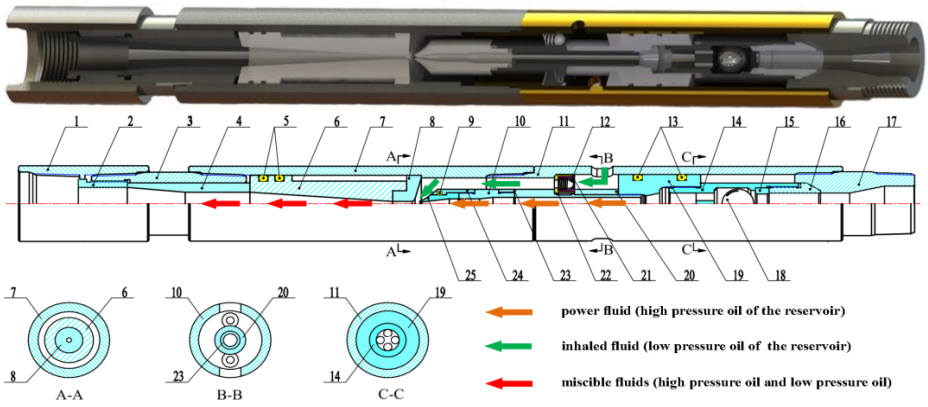

Figure 2. The structure and working principle of the new jet pump: 1. tubing clamp; 2. compression bolt; 3. tubing connector; 4. expanded pipe; 5. seal ring A; 6. diffuser tube; 7. pump housing; 8. throat; 9. seal ring B; 10. center connector; 11. joint of pump housing; 12. valve disk; 13. seal ring C; 14. check valve block; 15. check valve seat; 16. seat gland; 17. tail tube; 18. steel ball; 19. joint pipe; 20. sleeve; 21. check valve with spring; 22. straight pin; 23. joint of valve disk; 24. nozzle holder; 25. nozzle holder.

This is a new type of jet pump that was designed to address the shortcomings of the existing technology, and the strata series of Shengli Oilfield and the energy of high-pressure reservoirs was used to realize the simultaneous extraction of high- and low-pressure reservoirs based on the Venturi jet principle. Compared with traditional jet pumps [7,16], this jet pump not only solves the existing problems of difficult fluid extraction and low oil-recovery efficiency in low-pressure reservoirs, but also better transforms the existing contradiction between layers; additionally, it avoids the production cost of injecting high-pressure fluid into a well and, thus, allows for lower costs and a higher efficiency. Thanks to its simple structure, good practicality, and high reliability, it also reduces the risk of underground accidents.

3. Establishment of Calculation Method and Simulation Model

3.1. Basic Governing Equations of Fluids

When high-pressure oil and low-pressure oil in reservoirs enter the new jet pump, although there are two kinds of fluids in the pump, there is only a single liquid phase. As the high-pressure oil is sprayed through the nozzle in the jet pump, the fluid velocity significantly increases and the pressure is high. At this time, the flow field in the jet pump should be regarded as the incompressible turbulent flow field and the flow of oil in the pump should also follow the Navier–Stokes equation in fluid mechanics; thus, the following continuity equation can be established in the Euler coordinate system [33,34]:

$$\frac{\partial \rho}{\partial t} + \frac{\partial(\rho u_x)}{\partial x} + \frac{\partial(\rho u_y)}{\partial y} + \frac{\partial(\rho u_z)}{\partial z} = 0 \tag{1}$$

where ρ is the density of the fluid (kg/m^3); t is time (s); and u_x, u_y, and u_z are the velocity components of the fluid microelement along the X, Y, and Z axes, respectively (m/s).

The momentum equation [32]:

$$\begin{cases} \rho \frac{du}{dt} = -\frac{\partial P_0}{\partial x} + \frac{\partial \tau_{xx}}{\partial x} + \frac{\partial \tau_{yz}}{\partial y} + \frac{\partial \tau_{zx}}{\partial z} + \rho f_x \\ \rho \frac{dv}{dt} = -\frac{\partial P_0}{\partial y} + \frac{\partial \tau_{yy}}{\partial x} + \frac{\partial \tau_{zy}}{\partial y} + \frac{\partial \tau_{xy}}{\partial z} + \rho f_y \\ \rho \frac{dw}{dt} = -\frac{\partial P_0}{\partial z} + \frac{\partial \tau_{zz}}{\partial x} + \frac{\partial \tau_{yz}}{\partial y} + \frac{\partial \tau_{xz}}{\partial z} + \rho f_z \end{cases} \tag{2}$$

where P_0 is the static pressure (Pa); τ_{ij} is the stress tensor (i and j can be taken as x, y, and z) (Pa); and f_k is the volume force of gravity (k can be taken as x, y, and z) (N/m^3).

3.2. Choice of Turbulence Model

The oil flow in the new jet pump is turbulent flow. In order to select the most suitable turbulence model for the jet pump to improve the simulation accuracy of the flow field, the overall structure of the new jet pump and the applicable conditions of the turbulence model were carefully analyzed. Since the jet pump contains the nozzle jet flow and the boundary layer flow, the realizable k–ε turbulence model cannot only accurately predict the divergence ratio of flat and cylindrical jets, but it is also suitable for boundary layer flow and flow separation. Therefore, we ultimately selected the turbulence model as the realizable k–ε model in this paper (in case there is a need to learn about the process in order to directly verify the numerical model, [32] can be referred to for reference). The equation of the turbulence model is:

$$\frac{\partial}{\partial t}(\rho k) + \frac{\partial}{\partial x_i}(\rho k u_j) = \frac{\partial}{\partial x_i}\left[\left(\mu + \frac{\mu_t}{\sigma_k}\right)\frac{\partial k}{\partial x_j}\right] + G_k + G_b - \rho\varepsilon - Y_M + S_k \quad (3)$$

$$\frac{\partial}{\partial t}(\rho \varepsilon) + \frac{\partial}{\partial x_j}(\rho \varepsilon u_j) = \frac{\partial}{\partial x_j}\left[\left(\mu + \frac{\mu_t}{\sigma_k}\right)\frac{\partial \varepsilon}{\partial x_j}\right] + \rho C_\varepsilon S_\varepsilon - \rho C_2 \frac{\varepsilon^2}{k + \sqrt{v\varepsilon}} + C_1 \frac{\varepsilon}{k} C_3 G_b + S_\varepsilon \quad (4)$$

where k is the turbulence kinetic energy (m^2/s^2); u_j is the velocity of the fluid (m/s); ε is the turbulent dissipation rate (m^2/s^3); μ is the dynamic viscosity of turbulence (Pa·s); G_k is the turbulent kinetic energy caused by the velocity gradient of the laminar flow (m^2/s^2); G_b is the turbulent kinetic energy caused by buoyancy (m^2/s^2); Y_M is the term that contributes to turning the dissipation rate of the turbulent pulsating expansion into the global flow field in the compressible flow; C_1, C_2, and C_3 are three constants; σ_ε and σ_k are the Prandtl numbers; and S_k and S_ε are user-defined source items.

3.3. Calculation Formula of Pump Efficiency

The evaluation of jet pump performance is mainly reflected by pump efficiency. After reviewing the literature [31], we found that the key components of jet pumps are not standardized; if differently sized jet pump components are selected, their working characteristics will be different. In the analysis of their working characteristics, dimensionless parameters are selected to describe characteristics of a jet pump; therefore, the specific calculation formula of pump efficiency is:

$$\eta = q\frac{p}{1-p} \quad (5)$$

$$q = \frac{q_2}{q_1} \quad (6)$$

$$p = \frac{p_d - p_s}{p_n - p_s} \quad (7)$$

where η is the efficiency of the new jet pump; q is the flow ratio; p is the pressure ratio; q_1 is the volume flow rate of power fluid (m^3/s); q_2 is the volume flow rate of the intake fluid (m^3/s); p_d is the pressure at the outlet of the diffuser tube (Pa); p_s is the pressure at the inlet of the intake fluid (Pa); and p_n is the pressure at the inlet of the power fluid (Pa).

3.4. Basic Characteristic Equation of Jet Pump

The basic characteristic equation of a jet pump aims to determine the relationship between the pressure, flow rate, and geometric dimensions of the pump. This paper used a momentum equation, an energy equation (Bernoulli equation), and an equation of continuity to derive the basic characteristic equation of the new jet pump (the derivation

process is tedious, and thus, it is omitted here, but it is described in detail in [32]). This equation provided an important basis for the theoretical research, structural design, and manufacturing of the current jet pump. Its specific form is:

$$N = \varphi_1^2 \left[\frac{2\varphi_2}{\mathrm{m}} + \left(2\varphi_2 - \frac{\mathrm{r}}{\varphi_4^2} \right) \frac{\rho q^2 \mathrm{r}}{\mathrm{m}^2} - \left(2 - \varphi_3^2 \right)(1 + \rho q) \frac{(1+q)}{\mathrm{m}^2} \right] \tag{8}$$

$$\rho = \frac{\rho_2}{\rho_1} \tag{9}$$

where N is the water head ratio, which is about equal to p; φ_1, φ_2, φ_3, and φ_4 are velocity coefficients [16] that are related to the surface roughness of the internal flow road in the jet pump (generally, the value of φ_1 is 0.975, the value of φ_2 is 0.975, the value of φ_3 is 0.925, and the value of φ_4 is 0.85) and whose values are determined empirically; m is the ratio between the area at the inlet of the throat and the area at the outlet of the nozzle in the new jet pump; r is the ratio between the area at the inlet of the throat and the area at the inlet of the throat minus the area at the outlet of the nozzle in the new jet pump; ρ is the ratio of the intake fluid density to power fluid density; ρ_2 is the density of the intake fluid; and ρ_1 is the density of the power fluid.

In order to verify the basic characteristic equation, the equation was compared with Zou's equation [35]. It can be seen in Figure 3 that the flow rate of our equation is smaller and that the fitted pump efficiency curves of the two equations almost coincide. As the flow ratio continues to increase, the deviation between the highest pump efficiency is always less than 5% and the overall trend of the two is almost the same, with certain deviations. Thus, the correctness of the basic characteristic equation in this paper was proven. The fundamental difference between the Zou equation and Equation (8) depends on the selection of the friction loss coefficient and different derivation formulas. If the flow ratio is small, the friction loss coefficient would have a slight influence on the results of the equation; thus, the calculated pump efficiency would be almost the same. Once the flow ratio increases, the pump efficiency from the equation with a large friction loss coefficient would be small, leading to a numerical difference.

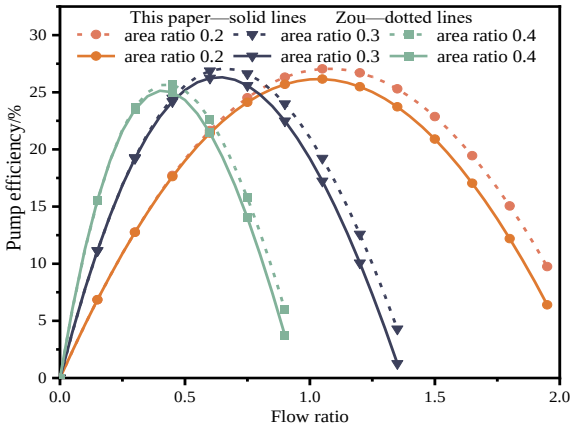

Figure 3. Verification of the basic characteristic equation.

After obtaining the basic characteristic equation of the new jet pump, we used MATLAB and the equation to draw the basic characteristic curve of the new jet pump. When the density of the power fluid and the intake fluid were the same (a density of 900 kg/m^3), the performance envelope curve of the new jet pump, as shown in Figure 4a, was obtained by changing the area ratio. It can be seen in the figure that in the case of a given area ratio, the pressure ratio gradually decreases with the increase in the flow ratio, whereas the pump efficiency first increases and then decreases, and there is a maximum efficiency value in each area ratio. With the increase in the area ratio, the maximum efficiency values of these different area ratios also first increase and then decrease. This conclusion is basically

consistent with previous conclusions in the literature [35]. It can be seen that both the area ratio and the flow ratio have a significant influence on pump efficiency.

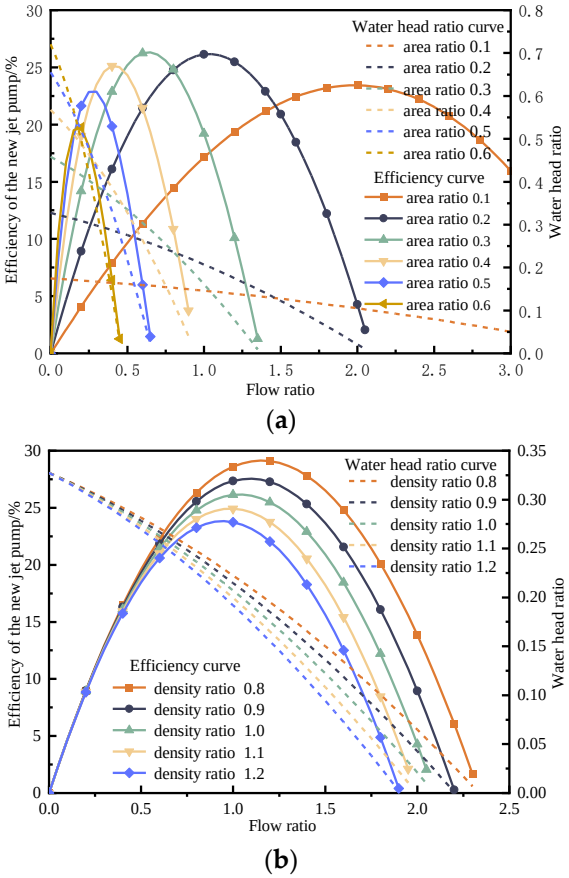

Figure 4. Performance envelope curve of the new jet pump. (**a**) Performance envelope curves of the new jet pump with different area ratios. (**b**) Performance envelope curves of the new jet pump at different density ratios.

The performance envelope curve of the new jet pump, as shown in Figure 4b, was obtained by changing the density ratio. It can be seen in the figure that in the case of a certain area ratio, the pressure ratio gradually decreases with the increase in the flow ratio, whereas the pump efficiency first increases and then decreases, and there is a maximum efficiency value at different density ratios. With the increase in the area ratio, the flow ratio corresponding to the highest efficiency value and the highest pump efficiency value of different density ratios gradually decreases, which indicates that the density ratio has a significant influence on the pump efficiency. This conclusion is also basically consistent with previous conclusions in the literature [16].

3.5. Establishment of a Simulation Model of the New Jet Pump

Due to the complex internal structure of the new jet pump, the three-dimensional modeling software SolidWorks and the numerical simulation software Fluent were used to establish the geometric model of the internal flow channel of the new jet pump. In order to improve the accuracy of the simulation results, the model was constructed according to a ratio of 1:1 (the whole process of modeling and simulation of the new jet pump is complicated, and thus, it is only briefly described here, but the whole process of the simulation was described in detail in [32]). The specific structure of the simulation model is shown in Figure 5; because subsequent meshing leads to poor mesh quality due to the complexity of the model, the simulation model was divided into two parts (simulation model a and simulation model b). It can be seen in the figure that a total of eight boundary

conditions were set in the simulation model: three inlet boundaries (Inlet 1, Inlet 2, and Inlet 3), one outlet boundary (Outlet), two boundaries of the interface (Interface 1 and Interface 2; the interface was mainly used for processing the data transfer between interfacial surfaces in the multizone calculation model), and two wall boundaries (Wall 1 and Wall 2). During simulation, the two boundaries of the interface are in contact; Wall 1 refers to all the remaining surfaces that are not defined in simulation model b, and Wall 2 refers to all the remaining surfaces that are not defined in simulation model a.

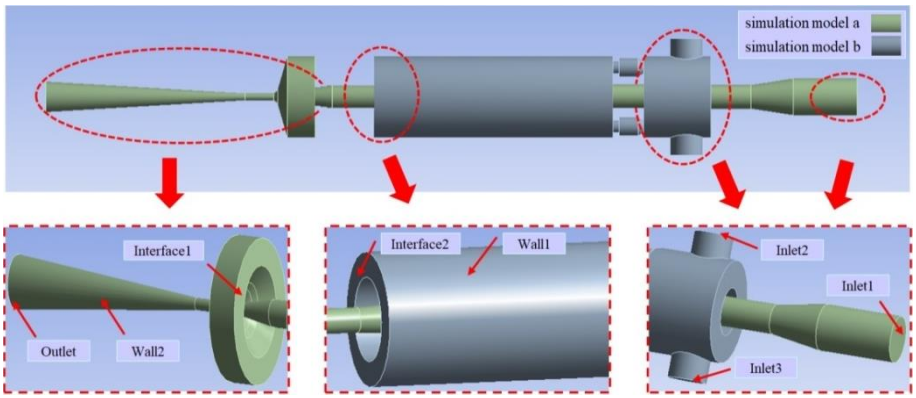

Figure 5. Simulation model of the new jet pump.

Based on actual conditions, our calculations showed that the inflow rate of power fluid was about 4.28 kg/s, the inflow rate of suction fluid was about 1.28 kg/s, and the outlet pressure of the jet pump was about 22.45 MPa. Therefore, we set Inlet 1 as the mass-flow inlet boundaries of the power liquid (4.28 kg/s), Inlet 2 and Inlet 3 as the mass-flow inlet boundary of the suction liquid (0.64 kg/s), and Outlet as the pressure outlet boundary of the jet pump (22.45 MPa). For the inlet boundary Inlet 1, we set the turbulence intensity as 5% and the hydraulic diameter as 5.22 mm. For the inlet boundaries Inlet 2 and Inlet 3, we set the turbulence intensity as 3% and the hydraulic diameter as 14 mm. For the outlet boundary Outlet, we set the turbulence intensity as 3% and the hydraulic diameter as 32 mm.

4. Meshing and Convergence Analysis of Simulation Model

When the simulation model of the new jet pump was meshed, in order to further improve the computational accuracy of the CFD (computational fluid dynamics) and effectively reduce the computational time of the numerical simulation, the influence of different mesh sizes on the simulation results was analyzed by changing the mesh size. (The simulation model was divided into mixed grids instead of single grids due to the complex simulation model. Therefore, the influence of the geometrical shape of single grids on the solution time and the accuracy of results are not discussed here. Because the two interfacial surfaces were circular, they were divided into hexahedral grids to process the data transfer between interfacial surfaces in the multizone calculation model.) It can be seen in Table 1 that a total of seven mesh partitioning methods were selected, and after comparing and analyzing the simulation results of these methods, it was found that the pressure value of the power fluid at Inlet 1 was almost the same when the grid sizes in the model were 1 mm and 2 mm, and the pressure values of these seven methods fluctuated between 36.89 MPa and 37.31 MPa. The simulation results not only verified the mesh independence of the model, but also showed that the convergence of the simulation results was good. In order to better improve the accuracy of the simulation results and minimize the computational time of the numerical simulation, the third mesh partition method was used to partition the simulation model.

Table 1. Grid independence verification of simulation model.

Meshing Method	Meshing Size (mm)	Number of Grid Nodes	Total Number of Units	Pressure of the Power Fluid at Inlet 1 (MPa)
#1	1	2,219,303	12,580,271	36.89
#2	1.5	670,295	3,693,996	37.01
#3	2	291,678	1,566,177	36.90
#4	2.5	154,344	807,660	37.08
#5	3	91,142	465,920	37.17
#6	3.5	58,893	294,429	37.26
#7	4	40,866	199,317	37.31

To verify the accuracy of the simulation results, the simulated pressure values of the power fluid inlet and two intake fluid inlets were extracted, and then the simulation results were compared with the theoretical calculation data one by one. It can be seen in Table 2 that the numerical difference between the simulated pressure value and the theoretical pressure value was only 2.88 MPa, and the relative error between them was only 8.4%. The simulated pressure value and the theoretical pressure value of the intake liquid inlets were also very close, and the average relative error between them was only 7.8%. The relative errors were all less than 10%, which not only indicated the correctness of the numerical simulation, but also further proved the accuracy of the simulation results.

Table 2. Verification of the accuracy of simulation results.

Locations	Theoretical Pressure Values (MPa)	Simulated Pressure Values (MPa)	Relative Errors (%)
Pressure of the power fluid at Inlet 1	34.02	36.90	8.4
Pressure of the intake fluid at Inlet 2	10	10.79	7.6
Pressure of the intake fluid at Inlet 3	10	10.84	8.0

5. Analysis of Influencing Factors of Pump Efficiency

The structure size and fluid physical characteristics have a significant influence on the efficiency of a jet pump. In order to better improve the efficiency of the new jet pump in the exploitation of high- and low-pressure reservoirs, based on the actual working conditions of the field, a numerical simulation analysis of the jet pump was carried out. The key structural parameters of the new jet pump are shown in Table 3. After the density of high-pressure oil was set to 900 kg/m^3 and that of low-pressure oil was set to 850 kg/m^3, the control variable method was used to analyze the influence of the throat–nozzle distance, the area ratio, and the length–diameter ratio of the throat on the efficiency of the jet pump and the flow field in the pump. Then, the optimal numerical intervals of the key structural parameters were obtained when the efficiency of the jet pump was at its maximum.

Table 3. Specific parameter values of key structures in the new jet pump.

Main Parameter Names	Units	Numerical Values
The number of the nozzle		1
Diameter of the nozzle outlet	mm	5.22
Diameter of the nozzle inlet	mm	15
Length of the throat at the nozzle outlet	mm	2.61
The convergence angle	°	14
Diameter of the throat	mm	6.65
Length of the throat	mm	40
Throat–nozzle distance	mm	10.44
Angle of the diffuser tube	°	8
Length of the diffuser tube	mm	167

5.1. Effect of the Throat–Nozzle Distance on Pump Efficiency

Low-pressure oil is carried by high-pressure oil between the nozzle outlet and the throat inlet; thus, the throat–nozzle distance has a significant influence on the suction range of high-pressure oil. After consulting the literature [8,21,36], it was found that the throat–nozzle distance is one of the main factors affecting pump efficiency. Therefore, the influence of different throat–nozzle distances on pump efficiency was studied by changing this distance. As shown in Table 4, when the throat–nozzle distances were 2.61 mm (0.5 times the diameter of the nozzle outlet) and 5.22 mm (the same as the diameter of the nozzle outlet), the pump efficiency was above 29%, and it can be seen in the figure that the range of the throat–nozzle distance that allowed for the maximum pump efficiency was between 2.61 mm and 5.22 mm. As the throat–nozzle distance continued to increase, the pump efficiency gradually and obviously decreased. When the throat–nozzle distance was 13.05 mm (2.5 times the diameter of the nozzle outlet), the pump efficiency was only about 20%, which further proved that the throat–nozzle distance was one of the main factors affecting the pump efficiency. Under the same working conditions, because the flow ratio did not change, the water head ratio curve showed the same trend as the pump efficiency curve (this conclusion can be obtained by analyzing Equation (5)).

Table 4. Effect of different throat–nozzle distances on pump efficiency.

Diameter of Nozzle Outlet (mm)	Distance from the Throat to Nozzle (mm)	Flow Ratio	Water Head Ratio	Pump Efficiency (%)
5.22	2.61	0.3156	0.4802	29.15
5.22	5.22	0.3156	0.4789	29.01
5.22	7.83	0.3156	0.4379	24.58
5.22	10.44	0.3156	0.4263	23.45
5.22	13.05	0.3156	0.3906	20.23
5.22	15.66	0.3156	0.3633	18.01

By extracting the velocity from the nozzle exit to the throat entrance of the new jet pump, as shown in Figure 6, we found that the maximum velocity at the nozzle outlet always fluctuated between 239 m/s and 247 m/s, the throat–nozzle distance gradually increased, and the size of the region with the highest fluid velocity (the red region) gradually decreased (this conclusion is basically consistent with the numerical simulation results in [35], which further proves the correctness of the numerical simulation in this paper). When the throat–nozzle distance was 3 times the diameter of the nozzle outlet, it could be clearly seen that only a small amount of high-speed fluid entered the throat. The reason for this result is that as the throat–nozzle distance gradually increased, the effective action distance for carrying the intake fluid became longer due to the power fluid and the velocity of the fluid was significantly reduced before it entered the throat.

5.2. Effect of Area Ratio on Pump Efficiency

The area ratio refers to the ratio of the inlet area of the throat to the outlet area of the nozzle. The area ratio should generally be greater than 1; if the area ratio is too small, it will cause serious wear to the inner wall of the jet pump, and if the area ratio is too large, there will be some liquid reflux. After consulting the literature [11,37], it was found that the area ratio is an important geometric parameter of jet pumps and that its value directly affects jet pump performance. Therefore, the influence of different area ratios on pump efficiency was studied by changing the diameter of the venture. Table 5 shows that when the diameter of the throat increased from 6.393 mm (area ratio of 1.5) to 7.382 mm (area ratio of 2), the efficiency of the jet pump gradually increased, but once the area ratio exceeded 2, the pump efficiency gradually decreased. It can be seen in the figure that the range of the diameter of the throat with maximum pump efficiency was between 6.39 mm and 8.25 mm. Under the same working conditions, the flow ratio did not change; thus, the water head ratio curve had the same trend as the pump efficiency curve.

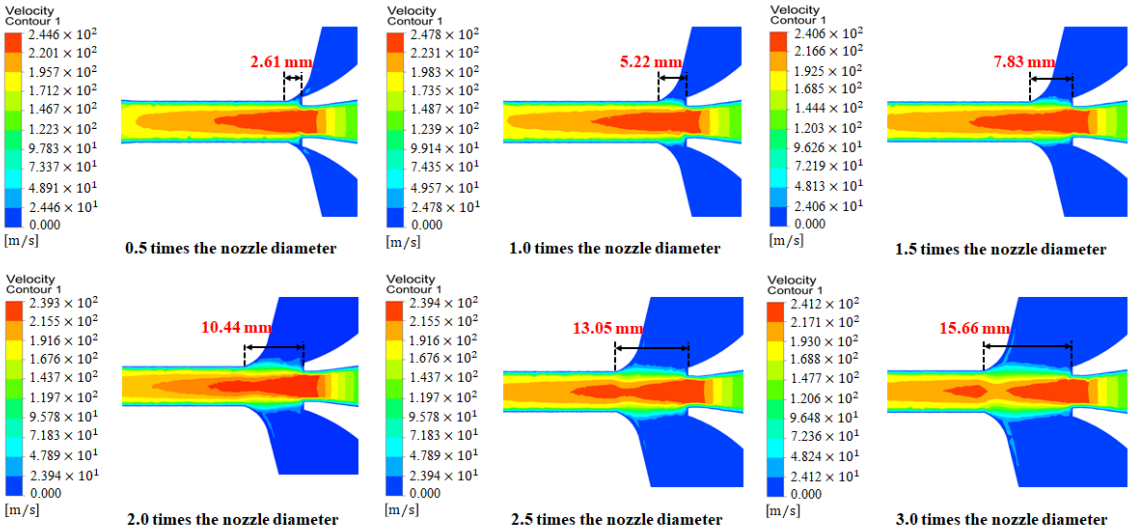

Figure 6. Velocity cloud diagrams from the nozzle outlet to the throat inlet with different throat–nozzle distances.

Table 5. Effect of different area ratios on pump efficiency.

Diameter of Nozzle Outlet (mm)	Diameter of Throat Inlet (mm)	Flow Ratio	Water Head Ratio	Pump Efficiency (%)
5.22	6.39	0.3156	0.4549	26.34
5.22	7.38	0.3156	0.4585	26.72
5.22	8.25	0.3156	0.4410	24.90
5.22	9.04	0.3156	0.404	21.39
5.22	9.77	0.3156	0.3599	17.74
5.22	10.44	0.3156	0.3215	14.95

By creating the velocity cloud diagrams of the throat outlet of the new jet pump with different throat diameters, as shown in Figure 7, it was found that when the throat diameter was 6.39 mm, the maximum velocity at the outlet was about 204 m/s and the velocity area was large, though there was a gradual increase in the diameter of the throat pipe. However, as the throat diameter gradually increased, the maximum velocity at the throat outlet gradually decreased, and as the area ratio gradually increased, the maximum velocity area gradually decreased (the conclusion of this numerical simulation was basically the same as that of the theoretical analysis in [11]). The reason for this result is that as the area ratio gradually increased, the sectional area at the throat outlet gradually increased and the contact area between the power fluid and the intake fluid in the throat also increased. These two parameters allow for a more adequate energy transfer in the throat tube, thus causing the maximum speed and the maximum speed area to gradually decrease with the increase in the area ratio.

5.3. Effect of the Throat Length–Diameter Ratio on Pump Efficiency

The throat is the main mixing area of the power and intake fluid, and the two carry out the main energy transfer in the throat; therefore, the throat length–diameter ratio has an important impact on the performance of a jet pump. After consulting the literature [11,38], it was found that the throat length–diameter ratio is one of the main factors affecting pump efficiency, and the throat length–diameter ratio of most jet pumps is greater than 4 and less than 10. Therefore, the influence of the throat length–diameter ratio on pump efficiency was studied by changing the length of the throat. As shown in Table 6, when the length of the throat was changed from 33.25 mm (where the throat length–diameter ratio was 5) to 46.55 mm (where the throat length–diameter ratio was 7), the pump efficiency gradually

increased. However, once the throat length–diameter ratio exceeded 7, the pump efficiency gradually decreased. It can be seen in the figure that the range of the length of the throat at maximum pump efficiency was between 39.3 mm (where the throat length–diameter ratio was 6) and 53.2 mm (where the throat length–diameter ratio was 8).

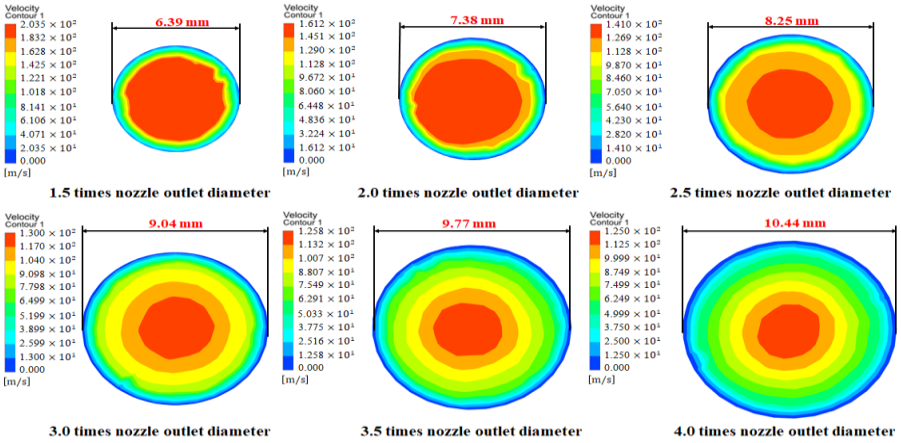

Figure 7. Velocity cloud diagrams of the throat outlet with different area ratios.

Table 6. Effect of different throat length–diameter ratios on pump efficiency.

Diameter of the Throat (mm)	Length of the Throat (mm)	Flow Ratio	Water Head Ratio	Pump Efficiency (%)
6.65	33.25	0.3156	0.4519	26.02
6.65	39.90	0.3156	0.4625	27.16
6.65	46.55	0.3156	0.4712	28.12
6.65	53.20	0.3156	0.4679	27.76
6.65	59.85	0.3156	0.4626	27.16
6.65	66.50	0.3156	0.4572	26.58

By extracting the velocity cloud diagrams of the throat outlet of the new jet pump with different throat length–diameter ratios, as shown in Figure 8, it was found that when the length of the throat was 33.25 mm, the maximum velocity at the outlet was about 134 m/s and the velocity area was small. However, as the length of the throat increased, the maximum velocity at the outlet of the throat gradually decreased, and when the length–diameter ratio gradually increased, the maximum velocity area gradually increased. The reason for this is that as the length–diameter ratio increased, the contact time between the power fluid and the intake fluid in the throat became longer, and thus, the power fluid and the intake fluid could allow for a more full energy transfer, causing the maximum velocity area to gradually increase with the increase in the length–diameter ratio.

5.4. Effect of Angle of the Diffuser Tube on Pump Efficiency

The function of the diffuser tube in a jet pump is to convert the kinetic energy of the mixed oil into pressure energy to lift the oil. After consulting the literature [11,39], it was found that the diffuser angle in the diffuser tube has a significant influence on the performance of jet pumps. Therefore, the influence of different diffuser angles on pump efficiency was studied by changing the diffuser angle. As shown in Table 7, when the diffuser angle was between 6° and 8°, the pump efficiency gradually increased with the increase in the diffuser angle. However, once the diffuser angle exceeded 8°, the pump efficiency gradually decreased with the increase in the diffuser angle. It can be seen in the figure that when the diffuser angle was 8°, the pump efficiency was at its maximum. The actual maximum pump efficiency was not reached at this point, but the range of the diffuser angle of the maximum pump efficiency was between 6° and 10°.

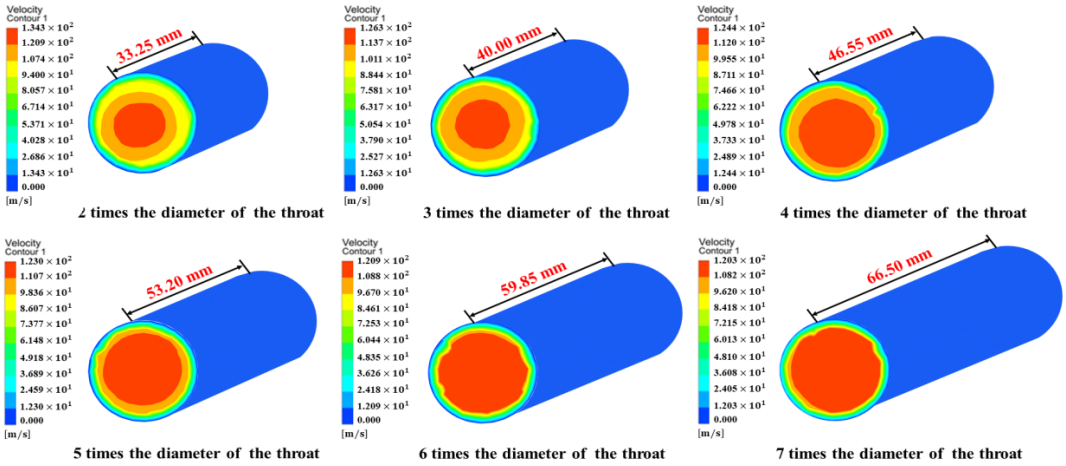

Figure 8. Velocity cloud diagrams of the throat outlet with different ratios of the length of the throat to its diameter.

Table 7. Effect of the different angles of the diffuser tube on pump efficiency.

Outlet Diameter of the Diffuser Tube (mm)	Angle of the Diffuser Tube (°)	Flow Ratio	Water Head Ratio	Pump Efficiency (%)
26.25	6	0.3156	0.4727	28.29
32.80	8	0.3156	0.4765	28.72
39.36	10	0.3156	0.4677	27.73
45.95	12	0.3156	0.4439	25.20
52.56	14	0.3156	0.4294	23.75
59.20	16	0.3156	0.4090	21.84

By extracting the velocity cloud diagrams from the diffuser tube of the new jet pump with different diffuser angles, as shown in Figure 9, it was found that the maximum velocity in the diffuser tube always fluctuated between 194 m/s and 196 m/s. When the diffuser angle was 6°, the miscible fluids could be fully developed for the entire section. The reason for this is that the fluid velocity was relatively fast, which increased the friction loss and caused the pump efficiency of the jet pump to decrease. As the diffuser angle increased, the velocity of miscible fluids decreased significantly less than the increase in the diffuser angle; thus, the velocity distribution surface in the diffuser tube did not fill the entire diffuser tube section. Thus, the performance of the new jet pump was significantly reduced (this conclusion is the same as that of the theoretical analysis in [35]).

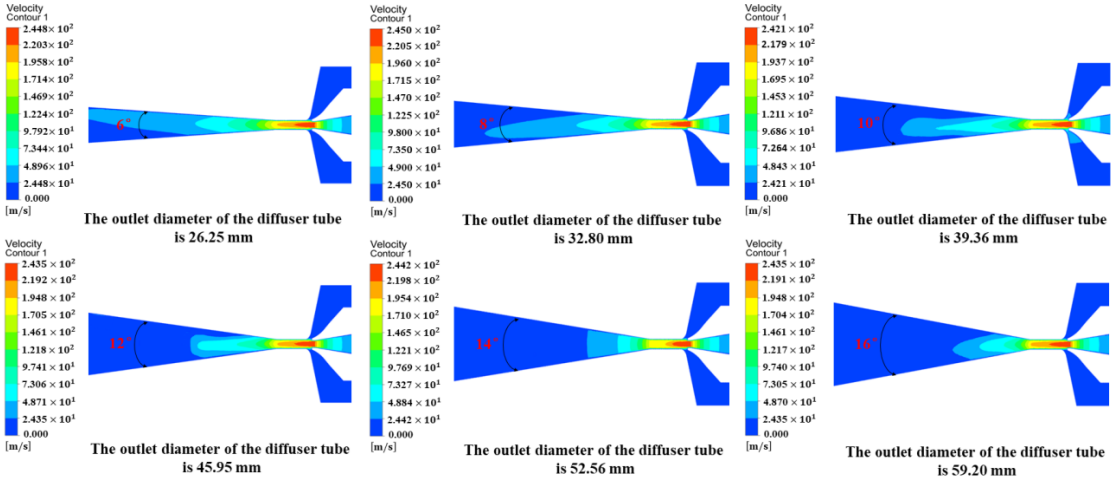

Figure 9. Velocity cloud diagrams of the diffuser tube with different diffuser angles.

5.5. Effect of the Flow Rate on the Pump Efficiency

Low-pressure oil is mixed with high-pressure oil in the throat to improve its speed and pressure; thus, the flow ratio is closely related to the mixing of the two fluids. After consulting the literature [11,40], it was found that the flow ratio is one of the main factors affecting pump efficiency. Therefore, the influence of the different flow rates on pump efficiency was studied by changing the volume flow of the power fluid. As shown in Table 8, when the power liquid flow was 0.45 (flow ratio of 0.2), the pressure ratio was at its maximum value, but the pump efficiency was less than 18%. As the flow ratio gradually increased, the pressure ratio began to decrease and the efficiency first increased and then decreased. It can be seen in the table that the range of the flow ratio of the maximum pump efficiency was 0.3 to 0.5.

Table 8. Effect of different flow rates on pump efficiency.

Flow of Intake Fluid (m^3/min)	Flow Ratio	Outlet Pressure of Diffuser Tube (MPa)	Water Head Ratio	Pump Efficiency (%)
0.09	0.2	22.45	0.4714	17.84
0.09	0.3	22.45	0.4449	24.04
0.09	0.4	22.45	0.3743	23.93
0.09	0.5	22.45	0.3224	23.79
0.09	0.6	22.45	0.2720	22.42
0.09	0.7	22.45	0.2210	19.86

By extracting the velocity cloud diagrams of the internal flow field in the jet pump with different flow ratios, as shown in Figure 10, it was found that when the flow ratio was 0.2, the maximum velocity of the power liquid at the nozzle outlet of the jet pump was 252 m/s, and as the flow ratio gradually increased, the maximum velocity at the nozzle outlet (the red area) gradually decreased (the conclusion of the numerical simulation is basically consistent with the theoretical analysis in [7]). The reason for this is that the volume flow of the intake fluid was a certain size; the volume flow of the power liquid gradually decreased with the increase in the flow ratio and the diameter of the nozzle outlet did not change; thus, the maximum velocity of the power fluid gradually decreased with the decrease in the volume flow of the power fluid.

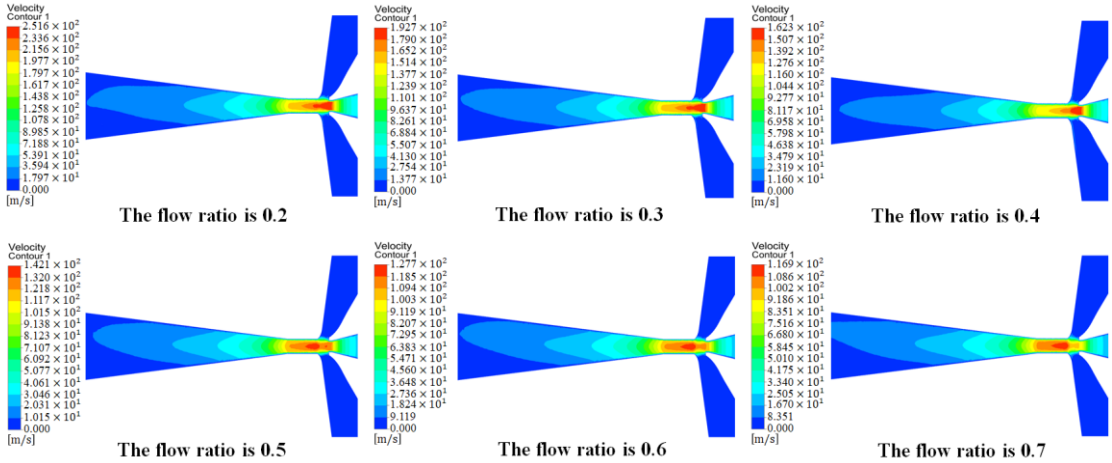

Figure 10. Velocity cloud diagrams of the flow field in the new jet pump with different flow ratios.

6. Structure Size Analysis of a New Jet Pump Based on the Taguchi Method

To achieve the lowest production costs and the shortest design and manufacturing time while maintaining customer satisfaction, Genichi Taguchi of Japan invented a robust design method that improved not only the quality of products, but also the research and development and design capabilities of domestic industries in Japan. This method is

commonly called the Taguchi method [41]. The specific implementation process of Taguchi's method (where the contents of the red-dashed box are the main steps) is shown in Figure 11, where the first step is to determine the test index, which directly reflects the quality of the product. Then, the test parameters that have the greatest impact on the test index are selected. The test parameters comprise two parts: the determination of control factors (the range and level of all control factors need to be determined) and the determination of noise factors (the internal and external noise factors need to be determined). After the test parameters are determined, the number of control factors and the number of levels are used to arrange the test plan. At this time, an orthogonal table needs to be constructed (the construction of the orthogonal table requires the use of relevant knowledge, such as probability theory [41]). According to the determined orthogonal table, the test is carried out, and the results are entered into the table. Then, range and S/N ratio analyses are used to determine the relative importance of each test parameter, and the variance is used to judge the relative influence of each factor on the target value in order to determine the best parameter scheme.

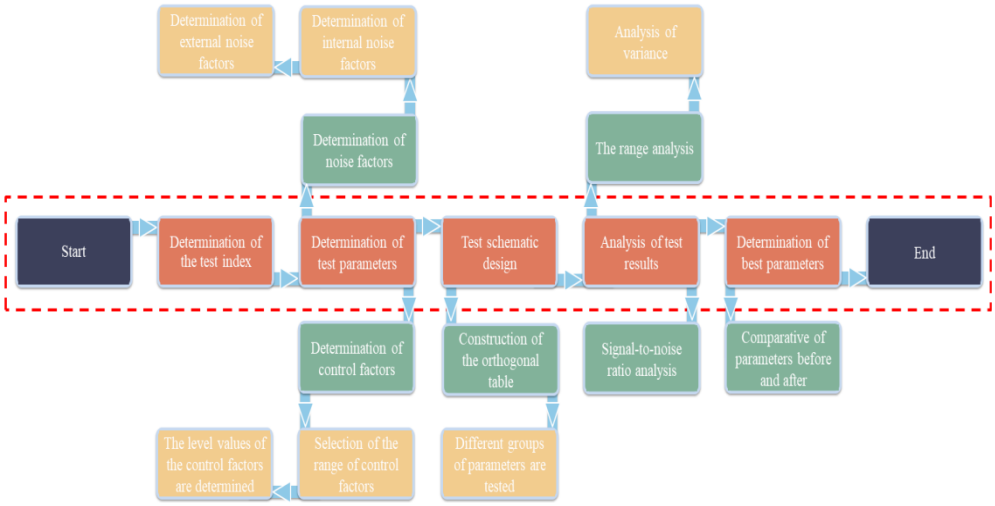

Figure 11. Implementation process of the Taguchi method.

6.1. Determination of the Test Index and Control Factors

The test index is the dependent variable in the test [42], and it mainly reflects the quality of the test results. The performance of a new jet pump is mainly reflected by the pump efficiency, and the value directly affects the production cycle and the current production cost. Here, the pump efficiency of the new jet pump was used as the test index.

Control factors are the independent variables in the test [42], and they must be considered when studying the test index. In general, a test index is mostly affected by multiple control factors; there are not only certain connections, but also significant differences between these control factors. By analyzing the abovementioned factors influencing pump efficiency, we found that the throat–nozzle distance, the diameter of the throat (area ratio), the length of the throat (throat length–diameter ratio), the diffuser angle, and the flow rate ratio have a significant influence on the pump efficiency because the power fluid flow and the intake fluid are not easy to control. Therefore, the throat–nozzle distance, the diameter of the throat, the length of the throat, and the diffuser angle were selected as control factors for Taguchi's method.

6.2. The Range and Level of the Control Factors

After the control factors were selected according to the optimal throat–nozzle distance interval, the diameter of the throat (area ratio) interval, the length of the throat (throat length–diameter ratio) interval, and the diffuser angle interval described above, the optimal range of the control factors from the Taguchi method was further determined. After the optimization of each control factor range was determined, it was necessary to design the

number of levels of control factors and the specific value of each level. The optimal range and specific values of control factors are shown in Table 9; it can be seen in the table that five levels were selected for each control factor, and the five levels of each control factor were equally distributed within the set optimal range.

Table 9. The range and level design of control factors.

The Control Factors	The Range of Factors	Level 1	Level 2	Level 3	Level 4	Level 5
Distance from the throat to nozzle (mm)	2.62~5.22	2.62	3.27	3.92	4.57	5.22
Diameter of the throat (mm)	6.4~8.0	6.4	6.8	7.2	7.6	8.0
Length of the throat (mm)	44~52	44	46	48	50	52
The diffuser angle (°)	6~9	6	6.75	7.5	8.25	9

6.3. Determination of Noise Factors

The test process was carried out using simulation software, and thus, there were no external noise factors. Although factors such as environment temperature, human operation errors, production errors, and other factors can be excluded in the process of finite element simulation, if the same model is divided into different mesh sizes, the final test index will also have a certain error caused by mesh division that can be used as an internal noise factor. To prevent the internal noise factors from influencing the final analysis results and to improve the accuracy of the test results, two mesh sizes (1 mm and 2 mm) with better convergence and higher accuracy were selected as described above; then, the simulation model was divided into these two mesh sizes, and the numerical simulation was carried out.

6.4. Construction of Orthogonal Tables and Orthogonal Tests

An orthogonal table is an essential tool for the Taguchi method. Such a table usually has two characteristics. The first is that the number of factor levels occurs with the same frequency in each column, and the second is that for all test groups, the level in one column has the same frequency of occurrence as the level in the other column. When a table satisfies both of these characteristics, it can be called an orthogonal table [43]. An orthogonal table and the results of these tests are shown in Table 10. Because the number of control factors in this test was 4, the level number of each control factor was 5. Additionally, the internal noise factor caused by grid division was also considered; therefore, a total of 50 tests were needed.

Table 10. Orthogonal table and the results of these tests.

Number	Distance from the Throat to the Nozzle	Diameter of the Throat	Length of the Throat	The Diffuser Angle	Pump Efficiency	
	(mm)	(mm)	(mm)	(°)	η_1 (%)	η_2 (%)
1	2.62	6.4	44	6	27.144	27.142
2	2.62	6.8	46	6.75	31.007	31.010
3	2.62	7.2	48	7.5	30.532	30.514
4	2.62	7.6	50	8.25	28.368	28.348
5	2.62	8	52	9	25.454	25.452
6	3.27	6.4	46	4.5	30.406	30.389
7	3.27	6.8	48	8.25	29.351	29.327
8	3.27	7.2	50	9	28.939	29.060
9	3.27	7.6	52	6	28.798	28.803
10	3.27	8	44	6.75	24.540	24.524
11	3.92	6.4	48	9	27.086	27.189
12	3.92	6.8	50	6	30.641	30.646
13	3.92	7.2	52	6.75	30.426	30.426
14	3.92	7.6	44	7.5	27.752	27.755
15	3.92	8	46	8.25	25.668	25.668
16	4.57	6.4	50	6.75	27.857	27.937
17	4.57	6.8	52	7.5	29.610	29.556

Table 10. *Cont.*

Number	Distance from the Throat to the Nozzle	Diameter of the Throat	Length of the Throat	The Diffuser Angle	Pump Efficiency	
	(mm)	(mm)	(mm)	(°)	η_1 (%)	η_2 (%)
18	4.57	7.2	44	8.25	28.293	28.324
19	4.57	7.6	46	9	25.660	25.702
20	4.57	8	48	6	25.455	25.431
21	5.22	6.4	52	8.25	25.899	25.942
22	5.22	6.8	44	9	27.970	28.084
23	5.22	7.2	46	6	29.270	29.435
24	5.22	7.6	48	6.75	26.852	26.944
25	5.22	8	50	7.5	25.431	25.453

6.5. Signal-to-Noise Ratio Analysis of Test Results

In order to better analyze the test results, the data in Table 5 were imported into the Minitab statistical software [43]. Since the software includes the Taguchi test module, the operation was easy and the analysis results were reliable. Generally speaking, the larger the signal-to-noise ratio, the better the quality, and when the delta of a parameter was large, this parameter had a significant influence on pump efficiency. It can be seen in Table 11 that the influencing factors of pump efficiency, from strong to weak, were the throat diameter, the diffuser angle, the throat–nozzle distance, and the length of the throat (the results obtained with this signal-to-noise ratio analysis are basically consistent with those obtained by other theoretical methods in [35]). For pump efficiency, bigger is better, and it can be seen in Figure 12 that when the throat–nozzle distance was level 1, the diameter of the throat was level 2, the length of the throat was level 2, and the diffuser angle was level 3 (i.e., the throat–nozzle distance was 2.62 mm, the diameter of the throat was 6.8 mm, the length of the throat was 46 mm, and the diffuser angle was 7.5°), the pump efficiency was at its maximum value.

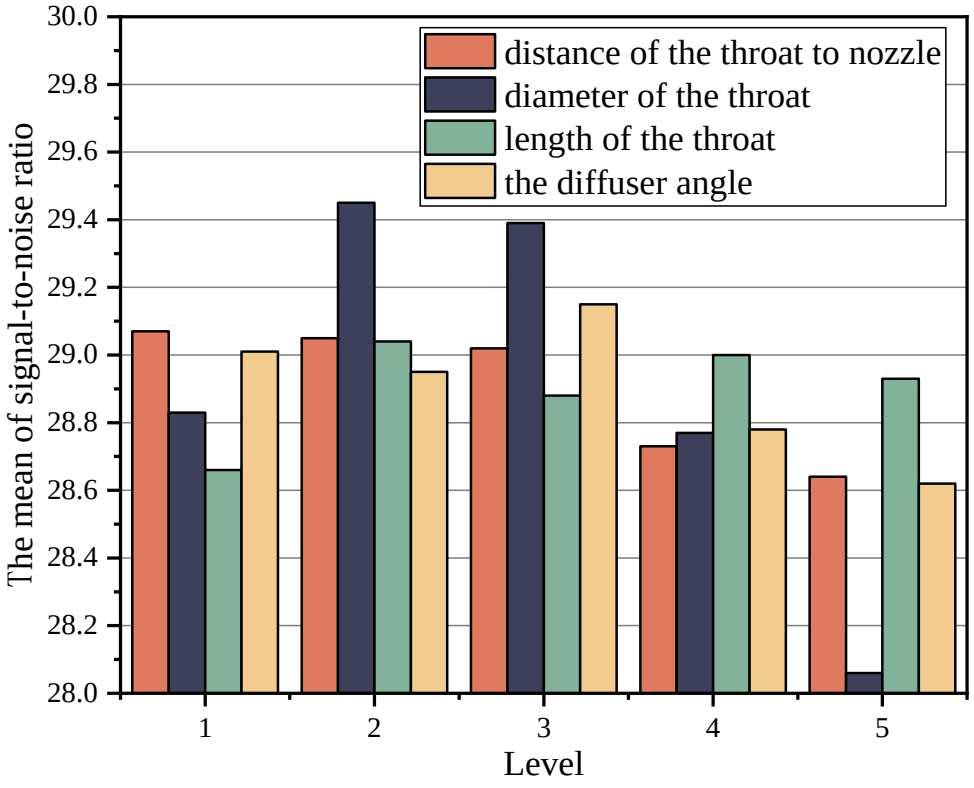

Figure 12. The main effect plot of the mean of the signal-to-noise ratio.

Table 11. S/N response table.

Level	Distance from the Throat to the Nozzle	Diameter of the Throat	Length of the Throat	The Diffuser Angle
	(mm)	(mm)	(mm)	(°)
1	29.07	28.83	28.66	29.01
2	29.05	29.45	29.04	28.95
3	29.02	29.39	28.88	29.15
4	28.73	28.77	29.00	28.78
5	28.64	28.06	28.93	28.62
Delta	0.43	1.39	0.38	0.53
Rank	3	1	4	2

6.6. Range Analysis of Test Results

After the Minitab statistical software was used to conduct the range analysis of the pump efficiency under each parameter combination in Table 10, a mean response table was obtained, as shown in Table 12. From this table, one can intuitively analyze the fluctuation between the pump efficiency and the level of each factor. By comparing the mean values and the rank of the mean values at different levels, it can be seen that the diameter of the throat had the greatest effect on pump efficiency, followed by the diffuser angle, the throat–nozzle distance, and the length of the throat. The optimal level of each factor was analyzed from the index effect, and it can be seen in Figure 13 that when the throat–nozzle distance of the new jet pump was level 1, the diameter of the throat was level 2, the length of the throat was level 2, and the diffuser angle was level 3, the pump efficiency reached its maximum value; this conclusion was consistent with the results of the signal-to-noise ratio analysis.

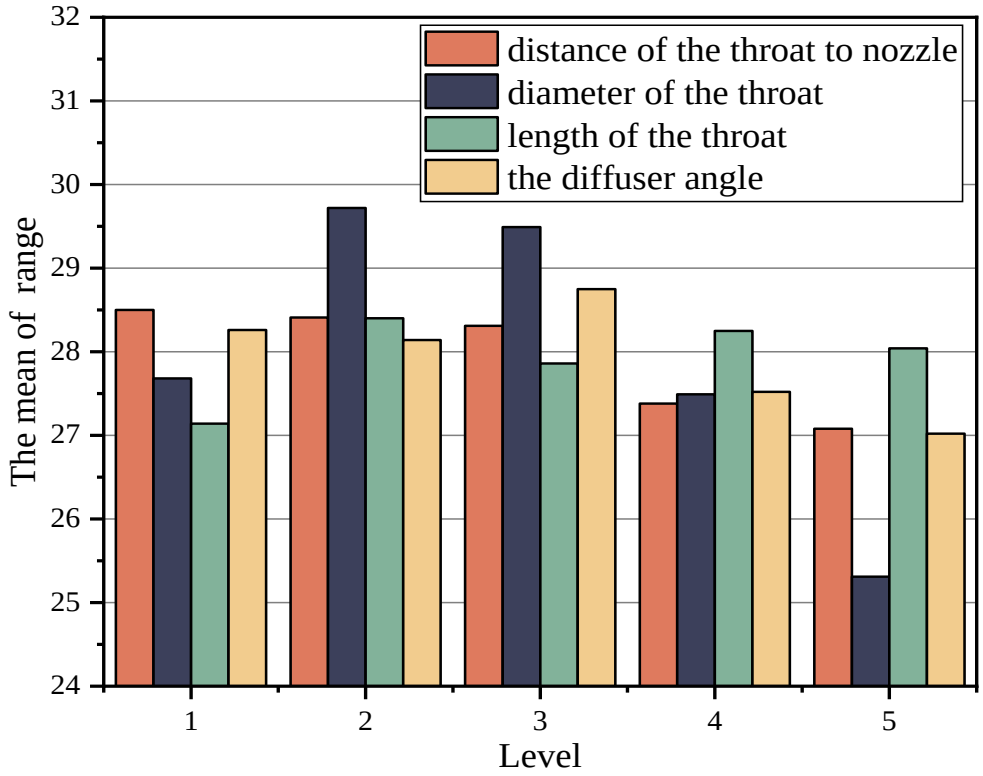

Figure 13. The main effect plot of the mean of the range.

Table 12. The mean response table.

Level	Distance from the Throat to the Nozzle	Diameter of the Throat	Length of the Throat	The Diffuser Angle
	(mm)	(mm)	(mm)	(°)
1	28.50	27.68	27.14	28.26
2	28.41	29.72	28.40	28.14
3	28.31	29.49	27.86	28.75
4	27.38	27.49	28.25	27.52
5	27.08	25.31	28.04	27.02
Delta	1.44	4.41	1.26	1.72
Rank	3	1	4	2

6.7. Variance Analysis of Test Results

In order to quantify the importance of the influence of the throat–nozzle distance, the throat diameter, the throat length, and the diffuser angle on pump efficiency, an analysis of variance was used to obtain the degree of freedom, the sum of squares, and the variance of each control factor. Then, the contribution degree of each control factor was calculated, and the relative influence degree of each control factor was determined. The results of the variance analysis of control factors are shown in Table 13; the degree of freedom in the table equals the total number of levels of each control factor minus 1. After determining the degree of freedom, the sum of squares, and other numerical values, we calculated the specific value of the variance and the F value (the value of F is the ratio of the variance of the control factor to the error variance). Then, each control factor's specific contribution to the pump efficiency of the new jet pump was obtained.

Table 13. Variance analysis of control factors.

Control Factors	Quadratic Sum	Degree of Freedom	Variance	Values of F	Contribution Degree
Distance from the throat to nozzle	0.766	4	0.192	1.721	9.12%
Diameter of the throat	6.378	4	1.595	14.293	75.93%
Length of the throat	0.446	4	0.112	1.004	5.31%
The diffuser angle	0.810	4	0.203	1.819	9.64%

It can be seen in Table 13 that the diameter of the throat contributed to a high degree, i.e., 75.93%, whereas the contribution of the other three was relatively small, and the degree of contribution of the throat–nozzle distance and the diffuser angle was similar. Comparing the two showed that the degree of influence of the diffuser angle on pump efficiency was slightly higher than that of the throat–nozzle distance. Among the four control factors, the contribution of the throat length was the lowest at 5.31%. Although the contributions of the throat–nozzle distance, the throat length, and the diffuser angle to the pump efficiency were not very high in this study, they are all important parameters that improve pump efficiency.

7. Comparative Analysis of the New Jet Pump before and after Optimization

The structure size, flow ratio, and pump efficiency of the new jet pump before and after optimization are compared in Table 14. It can be clearly seen that the throat–nozzle distance before optimization was much larger than that after optimization. The diameter and length of the throat after optimization were larger than those before optimization, but the diffuser angle after optimization was smaller than before optimization, and the difference between the two was only 0.5°. The new jet pump before optimization and the new jet pump after optimization were simulated under the condition of a certain flow ratio, and the pump efficiency of the new jet pump before and after optimization was calculated by using the pump efficiency calculation formula and the data derived from the numerical simulation. It was found that the pump efficiency before optimization was only 21.81%,

the pump efficiency after optimization was 31.26% (at present, the highest efficiency of a deep-well jet pump is less than 36% in practical applications [43]), and the difference between the pump efficiencies of the two was about 10%.

Table 14. Comparative analysis of the structure size and pump efficiency of the new jet pump before and after optimization.

The New Jet Pump	Distance from the Throat to the Nozzle	Diameter of the Throat	Length of the Throat	The Diffuser Angle	Flow Ratio	Pump Efficiency
	(mm)	(mm)	(mm)	(°)		(%)
Before optimization	10.44	6.65	40	8.0	0.3156	21.81
After optimization	2.62	6.80	46	7.5	0.3156	31.26

By comparing the velocity cloud diagrams of the new jet pump before and after optimization in Figure 14, it can be clearly seen that the maximum velocities of the fluid in the new jet pump before and after optimization were almost the same. The effective action distance of the intake fluid and of the power fluid became longer, and it can be seen that only a small part of the high-speed fluid (the red area) in the new jet pump before optimization entered the throat pipe. Although the difference in the diffuser angles before and after optimization was small, the mixed fluid in the latter could be fully developed for the entire cross-section. A comprehensive analysis of the data in Table 14 and Figure 14 proves that the new jet pump after optimization had a significant improvement in performance compared with that before optimization, and it is further shown that using the Taguchi method allowed us to optimize the structure size and improve the pump efficiency of the jet pump.

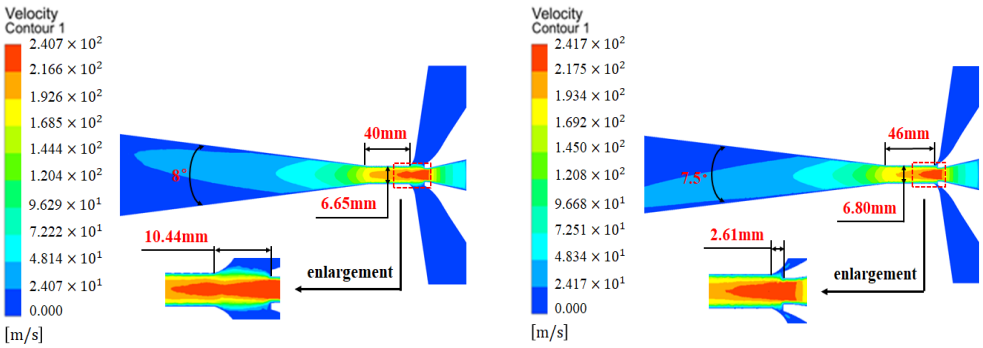

Figure 14. Velocity cloud diagram of the new jet pump before and after optimization. (**a**) Before optimization. (**b**) After optimization.

8. Conclusions

1. A new type of jet pump was designed to enhance the efficiency of oil recovery in wells in Eastern Shandong, China and to effectively exploit low-energy and low-yield zones. The jet pump simultaneously extracts oil from high- and low-pressure reservoirs by transforming the existing contradiction between layers in the well based on the Venturi jet principle. The method further lowers costs and enhances efficiency compared with traditional oil-recovery methods. Thanks to its simple structure, good practicality, and high reliability, the new jet pump also reduces the risk of underground safety accidents.
2. A new equation for the basic characteristics of the new jet pump was derived. A comparison of this new equation with the existing equations verified the correctness of this equation. According to the analysis of the envelope curve of the performance (drawn in the 2016 version of MATLAB using the derived equation of basic character-

istics) of the jet pump, the density ratio, flow rate ratio, and area ratio had a significant influence on pump efficiency; in addition, as the density ratio gradually increased, both the highest pumping efficiency among different density ratios and the flow ratio corresponding to the highest pumping efficiency gradually decreased.

3. According to an analysis of the internal flow field of the new jet pump, the increase in the throat–nozzle distance attenuated the flow core area because the effective action distance of the intake fluid being carried became longer due to the power fluid; thus, the velocity of the fluid was significantly reduced before it entered the throat. As the area ratio increased, both the maximum velocity at the throat outlet and the area of the maximum velocity gradually decreased (the reason for this is that as the area ratio gradually increased, the power fluid and the intake fluid carried out a more adequate energy transfer in the throat tube). An increase in the aspect ratio caused the maximum velocity area at the throat outlet to gradually increase (the reason for this is that the contact time between the power fluid and the intake fluid in the throat became longer, and therefore, the two could allow for a more full energy transfer). The increase in the diffuser angle resulted in the velocity distribution area in the diffuser tube not being able to cover the whole cross-section of the diffuser tube (the reason for this is that the velocity of miscible fluids decreased significantly less than the increase in the diffuser angle, which caused the velocity distribution surface in the diffuser tube to not fill the entire diffuser tube section).
4. To improve the pumping efficiency of the new jet pump in the extraction of high- and low-pressure reservoirs, its structural dimensions were optimized using the Taguchi method and numerical simulations (this is a new method for optimizing the structure of jet pumps). According to an analysis of the test results using signal-to-noise ratio and range analyses, the factors influencing pumping efficiency are, in descending order, the throat diameter, diffuser angle, throat–nozzle distance, and throat length. The contributions (relative influence on pumping efficiency) of these control factors were then obtained using an ANOVA. The throat diameter had the highest contribution (75.93%), followed by the diffuser angle (9.64%), throat–nozzle distance (9.12%), and throat length (5.31%).
5. The efficiency of the new jet pump was optimized with a combination of parameters including a level 1 throat–nozzle distance, a level 2 throat diameter, a level 2 throat length, and a level 3 diffuser angle (i.e., a throat–nozzle distance of 2.62 mm, a throat diameter of 6.8 mm, a throat length of 46 mm, and a diffuser angle of 7.5°). A comparison with the jet pump before optimization indicated that the pump efficiency was increased from 21.81% to 31.26%, further demonstrating a considerable improvement in the performance of the new jet pump.

Author Contributions: Methodology, Y.L.; software, J.W.; validation, Z.W. (Zhenhua Wu) and M.Z.; writing—original draft, Z.W. (Zhiliang Wang); funding acquisition, R.L. All authors have read and agreed to the published version of the manuscript.

Funding: This work was supported by the National Natural Science Foundation of China (No. 62173049).

Data Availability Statement: The datasets used and/or analyzed during the current study are available from the corresponding author upon reasonable request.

Conflicts of Interest: The authors declare no conflict of interest.

References

1. Wang, H.; Huang, H.; Bi, W.; Ji, G.; Zhou, B.; Zhuo, L. Deep and ultra-deep oil and gas well drilling technologies: Progress and prospect. *Nat. Gas Ind. B* **2022**, *9*, 141–157. [CrossRef]
2. Wu, X.; Wan, F.; Chen, Z.; Han, L.; Li, Z. Drilling and completion technologies for deep carbonate rocks in the Sichuan Basin: Practices and prospects. *Nat. Gas Ind. B* **2020**, *7*, 547–556. [CrossRef]
3. Bintarto, B.; Auliya, R.R.; Putra, R.A.M.; Pradipta, A.S.; Kurnia, R.A. Production Data Analysis and Sonolog for Determining Artificial Lift Design and Well Characteristic. *J. Pet. Geotherm. Technol.* **2020**, *1*, 28–35. [CrossRef]

4. Kolawole, O.; Gamadi, T.D.; Bullard, D. Artificial lift system applications in tight formations: The state of knowledge. *SPE Prod. Oper.* **2020**, *35*, 422–434. [CrossRef]
5. Clegg, J.; Bucaram, S.; Hein, N. Recommendations and Comparisons for Selecting Artificial-Lift Methods (includes associated papers 28645 and 29092). *J. Pet. Technol.* **1993**, *45*, 1128–1167. [CrossRef]
6. Holden, J. Fixing the Deep-Well Jet Pump. *Midwest Q.* **2009**, *50*, 357–359.
7. Zou, C.H.; Li, H.; Tang, P.; Xu, D.H. Effect of structural forms on the performance of a jet pump for a deep well jet pump. In Proceedings of the 17th International Conference on Computational Methods and Experimental Measurements, Opatija, Croatia, 5–7 May 2015.
8. Zhang, H.; Zou, D.; Yang, X.; Mou, J.; Zhou, Q.; Xu, M. Liquid–Gas Jet Pump: A Review. *Energies* **2022**, *15*, 6978. [CrossRef]
9. van der Lingen, T.W. A jet pump design theory. *J. Fluids Eng.* **1960**, *82*, 1128–1167. [CrossRef]
10. Mallela, R.; Chatterjee, D. Numerical investigation of the effect of geometry on the performance of a jet pump. *Proc. Inst. Mech. Eng. Part C J. Mech. Eng. Sci.* **2011**, *225*, 1614–1625. [CrossRef]
11. Lu, H.Y. *Theory and Application of Jet Technology*; Wuhan University Press: Wuhan, China, 2004.
12. Reddy, Y.R.; Kar, S. Theory and performance of water jet pump. *J. Hydraul. Div.* **1968**, *94*, 1261–1282. [CrossRef]
13. Cunningham, R.G. Gas compression with the liquid jet pump. *J. Fluids Eng.* **1974**, *96*, 203–215. [CrossRef]
14. Grupping, W.; Coppes, J.L.R.; Groot, J.G. Fundamentals of oil well jet pumping. *SPE Prod. Eng.* **1988**, *3*, 9–14. [CrossRef]
15. Winoto, S.H.; Li, H.; Shah, D.A. Efficiency of jet pumps. *J. Hydraul. Eng.* **2000**, *126*, 150–156. [CrossRef]
16. Wang, C.B. Research on the Jet Pumps Used in the Drain Sand of Petroleum Well. Ph.D. Thesis, Zhejiang University, Hangzhou, China, 2004. (In Chinese).
17. Kwon, O.B.; Kim, M.K.; Kwon, H.C.; Bae, D.S. Two-dimensional numerical simulations on the performance of an annular jet pump. *J. Vis.* **2002**, *5*, 21–28. [CrossRef]
18. Moghaddam, M.A.E.; Abandani, M.R.H.S.; Hosseinzadeh, K.; Shafii, M.B.; Ganji, G.G. Metal foam and fin implementation into a triple concentric tube heat exchanger over melting evolution. *Theor. Appl. Mech. Lett.* **2022**, *12*, 100332. [CrossRef]
19. Hosseinzadeh, K.; Moghaddam, M.A.E.; Asadi, A.; Mogharrebi, A.R.; Jafari, B.; Hasani, M.R.; Ganji, D.D. Effect of two different fins (longitudinal-tree like) and hybrid nano-particles (MoS2-TiO2) on solidification process in triplex latent heat thermal energy storage system. *Alex. Eng. J.* **2021**, *60*, 1967–1979. [CrossRef]
20. Yamazaki, Y.; Yamazaki, A.; Narabayashi, T.; Suzuki, J.; Shakouchi, T. Studies on mixing process and performance improvement of jet pumps (Effect of nozzle and throat shapes). *J. Fluid Sci. Technol.* **2007**, *2*, 238–247. [CrossRef]
21. Aldaş, K.; Yapıcı, R. Investigation of effects of scale and surface roughness on efficiency of water jet pumps using CFD. *Eng. Appl. Comput. Fluid Mech.* **2014**, *8*, 14–25. [CrossRef]
22. Xu, K.; Wang, G.; Zhang, L.; Wang, L.; Yun, F.; Sun, W.; Wang, X.; Chen, X. Multi-objective optimization of jet pump based on RBF neural network model. *J. Mar. Sci. Eng.* **2021**, *9*, 236. [CrossRef]
23. Chen, S.; Yang, D.; Zhang, Q.; Wang, J. An integrated sand cleanout system by employing jet pumps. *J. Can. Pet. Technol.* **2009**, *48*, 17–23. [CrossRef]
24. Gao, C.C.; Wang, X.H. Application of jet pump technology in environmental protection. *Environ. Prot. Sci.* **2009**, *35*, 11–14. (In Chinese)
25. Sarshar, S. The Recent Applications of Jet Pump Technology to Enhance Production from Tight Oil and Gas Fields. In Proceedings of the SPE Middle East Unconventional Gas Conference and Exhibition, Abu Dhabi, United Arab Emirates, 23–25 January 2012.
26. Sun, B. Study on Gas Production Technology of Coalbed Methane Jet Pump. Master's Thesis, Southwest Petroleum University, Chengdu, China, 2016. (In Chinese).
27. Chen, S.; Li, H.; Zhang, Q.; He, J.; Yang, D. Circulating usage of partial produced fluid as power fluid for jet pump in deep heavy-oil production. *SPE Prod. Oper.* **2007**, *22*, 50–58. [CrossRef]
28. Gazzar, M.E.; Meakhail, T.; Mikhail, S. Numerical study of flow inside an annular jet pump. *J. Thermophys. Heat Transf.* **2006**, *20*, 930–932. [CrossRef]
29. Kurkjian, A.L. Optimizing Jet-Pump Production in the Presence of Gas. *SPE Prod. Oper.* **2019**, *34*, 373–384. [CrossRef]
30. Samad, A.; Nizamuddin, M. Flow analyses inside jet pumps used for oil wells. *Int. J. Fluid Mach. Syst.* **2013**, *6*, 1–10. [CrossRef]
31. Sheha, A.A.A.; Nasr, M.; Hosien, M.A.; Wahba, E. Computational and experimental study on the water-jet pump performance. *J. Appl. Fluid Mech.* **2018**, *11*, 1013–1020. [CrossRef]
32. Wang, Z.L. Structure Design and Simulation Analysis of Jet Pump in High and Low Pressure Reservoir. Master's Thesis, Yangtze University, Jingzhou, China, 2022. (In Chinese).
33. Hosseinzadeh, K.; Moghaddam, M.A.E.; Asadi, A.; Mogharrebi, A.; Ganji, D. Effect of internal fins along with hybrid nano-particles on solid process in star shape triplex latent heat thermal energy storage system by numerical simulation. *Renew. Energy* **2020**, *154*, 497–507. [CrossRef]
34. Hosseinzadeh, K.; Mogharrebi, A.R.; Asadi, A.; Paikar, M.; Ganji, D. Effect of fin and hybrid nano-particles on solid process in hexagonal triplex latent heat thermal energy storage system. *J. Mol. Liq.* **2020**, *300*, 112347. [CrossRef]
35. Zou, M.M. Design and Analysis of Deep Well Jet Pump. Master's Thesis, Southwest Petroleum University, Chengdu, China, 2016. (In Chinese).
36. Lyu, Q.; Xiao, Z.; Zeng, Q.; Xiao, L.; Long, X. Implementation of design of experiment for structural optimization of annular jet pumps. *J. Mech. Sci. Technol.* **2016**, *30*, 585–592. [CrossRef]

37. Long, X.; Zhang, J.; Wang, Q.; Xiao, L.; Xu, M.; Lyu, Q.; Ji, B. Experimental investigation on the performance of jet pump cavitation reactor at different area ratios. *Exp. Therm. Fluid Sci.* **2016**, *78*, 309–321. [CrossRef]
38. Long, X.; Yan, H.; Zhang, S.; Yao, X. Numerical simulation for influence of throat length on annular jet pump performance. *J. Drain. Irrig. Mach. Eng.* **2010**, *28*, 198–201, 206. (In Chinese)
39. Liu, B.; Dong, S.; Tan, J.; Li, D.; Yang, J. Design and flow simulation of a micro steam jet pump. *Mod. Phys. Lett. B* **2022**, *36*, 2250018. [CrossRef]
40. Gan, J.; Zhang, K.; Wang, D. Research on Noise-Induced Characteristics of Unsteady Cavitation of a Jet Pump. *ACS Omega* **2022**, *7*, 12255–12267. [CrossRef] [PubMed]
41. Karna, S.K.; Sahai, R. An overview on Taguchi method. *Int. J. Eng. Math. Sci.* **2012**, *1*, 1–7.
42. Tsui, K.L. An overview of Taguchi method and newly developed statistical methods for robust design. *Iie Trans.* **1992**, *24*, 44–57. [CrossRef]
43. Mathews, P.G. *Design of Experiments with MINITAB*; ASQ Quality Press: Milwaukee, WI, USA, 2005.